

Chapter 2

Rheology of Shear Thickening Fluid



Miguel Montenegro, Laura Campo-Deaño, and Francisco J. Galindo-Rosales

Nomenclature

BET	Back extrusion technique
CST	Continuous shear thickening
CSR	Controlled shear rate
CSS	Controlled shear stress
DST	Discontinuous shear thickening
d_0	Initial diameter (m)
d_f	Final diameter (m)
d_{\min}	Minimum diameter (m)
F	Force (N)
g	Gravitational acceleration (m^2/s)
G'	Storage modulus (Pa)
G''	Loss modulus (Pa)
h_0	Initial height
L	Length (m)

M. Montenegro · L. Campo-Deaño

CEFT—Centro de Estudos de Fenómenos de Transporte, Departamento de Engenharia Mecânica, Faculdade de Engenharia da Universidade do Porto, Porto, Portugal

ALiCE—Laboratório Associado em Engenharia Química, Faculdade de Engenharia da Universidade do Porto, Porto, Portugal

F. J. Galindo-Rosales (✉)

ALiCE—Laboratório Associado em Engenharia Química, Faculdade de Engenharia da Universidade do Porto, Porto, Portugal

CEFT—Centro de Estudos de Fenómenos de Transporte, Departamento de Engenharia Química, Faculdade de Engenharia da Universidade do Porto, Porto, Portugal

e-mail: galindo@fe.up.pt

LAOS	Large amplitude oscillatory shear
LVR	Linear viscoelastic region
MRSTF	Magnetorheological shear thickening fluid
N_1	First normal stress difference
N_2	Second normal stress difference
PCC	Precipitated calcium carbonate
Q	Flow rate (m^3/s)
r	Radius (m)
SAOS	Small amplitude oscillatory shear
SBE	Short back extrusion
SHPB	Split-Hopkinson pressure bar
STF	Shear thickening fluid
t	Time (s)
wt	Mass fraction (%)
δ	Phase angle (rad)
Δp	Pressure drop (Pa)
γ	Strain
$\dot{\gamma}$	Shear rate (s^{-1})
$\dot{\gamma}_w$	Shear rate at wall (s^{-1})
$\dot{\epsilon}$	Extension rate (s^{-1})
η	Shear viscosity ($\text{Pa}\cdot\text{s}$)
η^+	Transient viscosity ($\text{Pa}\cdot\text{s}$)
Λ_0	Initial aspect ratio
ρ	Density (kg/m^3)
σ	Surface tension (N/m)
τ	Shear stress (Pa)
τ_w	Shear stress at wall (Pa)
Ψ_1^+	First normal stress coefficient
Ψ_2^+	Second normal stress coefficient
ω	Angular frequency (rad/s)

2.1 Introduction

Rheology is the field of science that studies the deformation and flow of complex materials [1]. A complex fluid is a sort of complex material that does not obey Newton's law of viscosity: it exhibits a nonlinear relationship between the imposed stress and the measured strain rate or vice versa [2]. In order to understand and model that relationship between stress and strain, we need to poke the material and observe how the material functions depend on the loading time scale, loading amplitude, external electromagnetic fields, temperature, etc. [3]. Rheometry is a branch of rheology dedicated to measuring the different material functions [4], which are determined under standard flows, such as shear and extensional flows that can provide complementary information to get a complete rheological characterization [5].

Shear thickening fluids (STFs) are complex fluids, typically consisting of dense suspensions of solid particles dispersed in an inert carrier fluid, that exhibit an increase in viscosity under the application of a shear rate/stress over a critical value [6]. In other words, the stress required to shear an STF increases faster than linearly with the shear rate [7], as shown in Fig. 2.1. In his seminal work of 1989 [10], Barnes stated that shear thickening behavior is normally conditioned by different parameters (Table 2.1). Subtle changes in the local particle arrangements are responsible for the transitions between shear thinning, Newtonian, and shear thickening regimes [9]. In recent years, it is common to distinguish between continuous shear thickening (CST) and discontinuous shear thickening (DST); the former is exhibited at intermediate packing fractions and the viscosity increase is relatively mild due to the formation of hydroclusters [11]; increasing the packing fraction, the viscosity increase becomes steeper up to a point where the viscosity exhibits a discontinuous increase beyond a critical shear rate, as result of the contact between particles [7].

Although shear thickening behavior may cause technical problems in flow processes, such as blockage of spraying nozzles or insufficient mold filling [12], thanks to their viscous dissipative nature and the possibility of tuning their viscosity curves, these fluids have allowed the development of important engineering solutions to different applications, namely in energy dissipation systems, such as vibration or impact absorption, which have accelerated in the last years [6, 13]. Even though STF has undergone dynamic loads in most of the applications, it is traditionally characterized by means of viscosity curves, which represent the equilibrium shear viscosity values reached at different steady shear rates. It is hard to believe that the STF will undergo steady simple shear flow in its final application, most probably the flow will be transient and complex, a combination of shear and extensional flows; this mismatch, both in terms of timescale and flow type, between the rheological

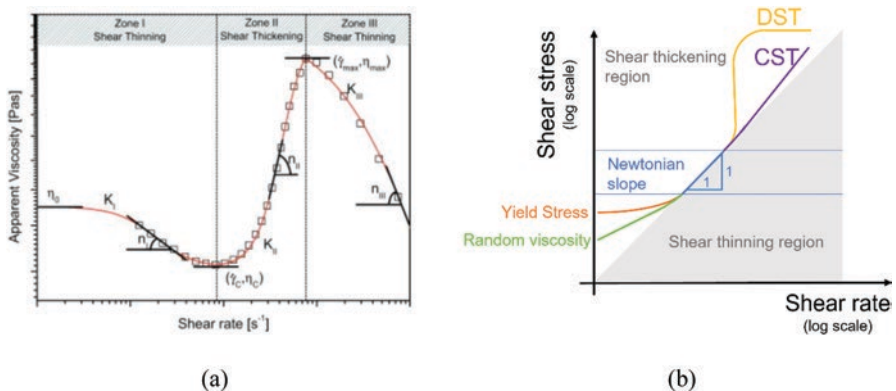


Fig. 2.1 (a) Sketch of a viscosity curve exhibited by STF transiting from Newtonian to shear thinning and shear thickening (CST) regimes [8]. (b) Sketch of different flow curves exhibiting CST and DST [9]. Reprinted by permission from Elsevier

Table 2.1 Parameters for conditioning the shear thickening behavior [10]

<i>Particle</i>	<ul style="list-style-type: none"> • Particle size • Particle size distribution • Particle shape • Particle-particle interaction • Volume fraction
<i>Continuous phase</i>	<ul style="list-style-type: none"> • Liquid phase viscosity
<i>Flow field</i>	<ul style="list-style-type: none"> • Type of deformation (shear or extension, steady or unsteady) • Rate of deformation • Time of deformation

information provided and the final deformation under real conditions, may result in a wrong performance of the fluid [14].

This chapter aims at providing a guide about how to perform a full rheological characterization of STF useful for both fitting and developing constitutive models and tweaking the formulations toward obtaining an optimal rheological performance of the fluid.

2.2 Shear Rheometry of STF

2.2.1 Steady Shear Flow

In shear rheometry, the fluid sample undergoes simple shear flow, which can be imposed either by rotational rheometers or by capillary (both at macro and microscales) ones [2]. Steady shear measurements allow obtaining either the viscosity curve, which provides information about the dependence of the steady shear viscosity on the shear rate, or the flow curve, which relates the steady shear stress with the shear viscosity.

There are two kinds of rotational rheometers: strain-controlled and stress-controlled rheometers, the latter commonly equipped with control systems allowing for operating in pseudo-strain-controlled mode. As highlighted by Mewis and Wagner [15], it is very important to bear in mind that “controlling stress allows one to move systematically through the transition, whereas in a strain-controlled device the discontinuous shear thickening region is generally not accessible”. Rotational rheometers enable the imposition of steady simple shear flow covering a wide range of shear rates/stresses by working with the right geometry, i.e., concentric cylinders, cone-plate or plate-plate, and the right dimensions. Whereas cone plate geometry ensures a homogeneous shear rate throughout the whole volume sample, for STF, plate-plate geometries are very convenient, particularly if wall slip would be an issue, as they can operate with grooved surfaces and different gaps to avoid it. Concentric cylinders can also be used with STF, as long as a small gap is being used to minimize the change of shear rate inside the gap and to avoid particle migration; however, loading a very viscous STF in a concentric cylinder geometry is more

difficult than in other rotational geometries [16, 17]. Some other precautions must be considered when working with STF, not because of its rheological behavior, but because STF mostly consists of a dense suspension of particles [15]: regarding the gap size, either operating with cone-plate or plate-plate geometry, it is of paramount importance ensuring that the ratio of gap size to particle/aggregate size is large enough, between 10 and 50; when the formulation consists of particles not neutrally buoyant with the carrier fluid and large enough to avoid the Brownian motion so that sedimentation dominates, a vertical concentration gradient will be developed and the top moving plate will “feel” an apparent reduction in the viscosity of the sample; as in many suspensions, some shear thickening samples may require a pre-shear protocol to ensure reproducibility in the measurements [18]; partial evaporation of the carrier fluid may be also an issue when working with volatile solvents, which can be avoided either by fractioning the range of shear rates to be covered in a single experiment or by reducing the shearing time at each shear rate.

The experimentalist is responsible for being aware of the instrument’s resolution, instrument inertia, sample inertia, boundary effects, and volumetric effects to avoid bad data [3] when operating the rotational rheometer. Working with STF, the maximum torque of the rheometer may be reached with ease if working with a cone-plate or plate-plate geometry. To avoid misinterpretations of the steady shear flow measurements, the experimental window must be properly identified, because the data set obtained below the minimum torque line can be misinterpreted as shear thinning behavior and data beyond the onset of secondary flows can be misunderstood as shear thickening behavior.

When performing steady shear flow measurements with STF in a rotational rheometer equipped with crosshatched, serrated, or grooved plates, it is important to perform several preliminary tests: the experimentalist should test different gap sizes in order to ensure that the measurements are gap independent [19], as the roughness of the plates may introduce gap dependency; surplus of material around the plates should be carefully trimmed, otherwise the presence of a few milliliters of suspension left on the bottom plate in contact with the paste between the two plates may strongly affect the critical shear rate and induce gap dependency [20].

Any complex fluid would be fully characterized under steady shear flow with three material functions [21], i.e., the variation with shear rate of the shear viscosity and the first and second normal stress differences, $N_1 = \sigma_{11} - \sigma_{22}$ and $N_2 = \sigma_{22} - \sigma_{33}$ respectively [22], where by convention 1, 2, and 3 are the velocity, velocity gradient, and vorticity directions, respectively, in a viscometric shear flow. For isotropic materials, N_1 has always been found to be positive (unless it is zero) and N_2 negative and smaller than N_1 in terms of magnitude [23]. If the material is an ideal solid (purely elastic), then the value of N_2 would be zero. Typically, a negative value of N_1 means that one is dealing with a shear thinning behavior. When dealing with STF, however, it has been found that the value of N_1 can also be negative and with an absolute value equal to the applied stress [24]. Andrade et al. [25] reported in their work that the transition from $N_1 \approx 0$ to a negative value of the first normal stress difference in their colloidal suspensions with DST behavior appeared at rates lower than the onset of the shear thickening regime and was also related to a lower volume

fraction, indicating contributions from lubrication forces, instead of the transition $N_1 \approx 0$ to positive (beyond critical shear rate) that suggested frictional interactions from contacts between particles. Pan et al. [26] also observed that increasing particle diameters in shear thickening granular suspensions led to the growing importance of hydrodynamic interactions, resulting in negative normal stresses. N_2 , however, generally remained very much neglected [27]; Laun [24] back in 1990s reported that $N_2 \approx -N_1/2$ in opposition to most of the reported measurements and numerical simulations [28]. Thus, as the measurement of both normal stress differences may be limited by capillary stresses as discussed by Brown and Jaeger [7, 29] and shown by Garland et al. [30], the information regarding the normal stresses can alternatively be obtained by means of extensional experiments.

Capillary rheometry has been typically used for determining the viscosity curves of polymer melts, providing reliable information at high shear rates, beyond the limits of rotational rheometers, and in similar conditions to the industrial process. The latter reasoning could be also applied to STF, as in many industrial processes, such as injection of pastes or ceramics inside molds, dense suspensions are extruded through a capillary and the shear thickening or jamming transition may happen in the process. The functioning principle of a capillary rheometer is very simple: the fluid sample flows at a controlled flow rate (Q) through a tube having a well-defined radius (r), and the pressure drop (Δp) between two points, within the fully developed region and separated by a certain distance (L), is measured. A non-slip condition is assumed to be held at the wall. As the shear rate at the wall ($\dot{\gamma}_w$) is directly proportional to the flow rate and the shear stress at the wall (τ_w) is also proportional to the pressure drop, the shear viscosity is just given by dividing one by the other ($\eta = \tau_w / \dot{\gamma}_w$). The basic principle of a capillary rheometer is illustrated in Fig. 2.2.

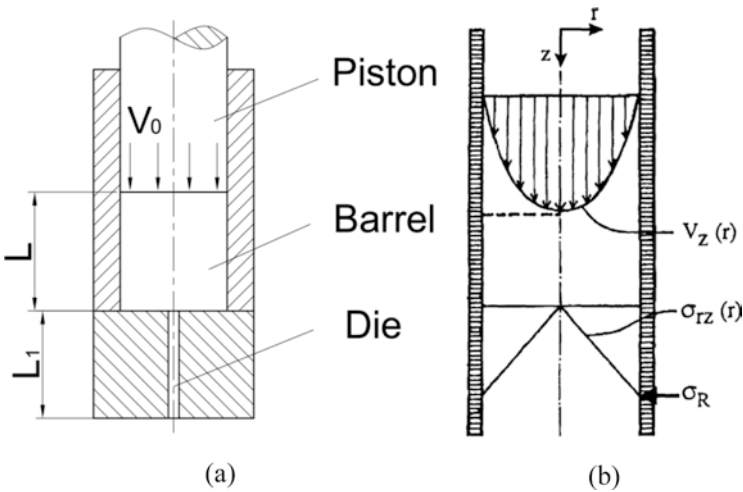


Fig. 2.2 (a) Schematic diagram of a high-pressure capillary rheometer [31]. (b) Velocity and shear stress profiles [32]. Reprinted by permission from Elsevier

This works well for Newtonian fluids; however, when dealing with shear thinning fluids, the Weissenberg-Rabinowitsch-Mooney (WRM) correction is required [23] because the shear rate at the wall is not linearly related to the flow rate. In principle, this correction also remains valid when working at the microscale with planar slit microfluidic devices [33]. However, the recent experimental results reported by Bossis and co-workers [34] discourage the use of capillary rheometry with STF, at least for those exhibiting DST. They realized that upon jamming, there is no longer a suspension flowing through a capillary, but instead a less concentrated suspension flows through a porous medium developed by the jammed particles; moreover, they also reported that the jamming does not occur inside the capillary but rather before its entrance, and finally, the fluctuations of pressure observed at constant shear rate are probably produced by the intermittent collapse of the jammed structure at the entrance of the die. However, they managed to get useful results [16] and, based on them, successfully modified the model proposed by Wyart and Cates [35]. Another interesting result from Bossis et al. [36] is that the jamming transition, which in the rotational rheometer occurs in a fraction of the inverse shear rate, exhibited in the extrusion a much slower dynamics than in the case of stress imposed on a rotational geometry. This latter observation supports the idea that characterizing STF under simple steady shear experiments in a rotational rheometer is by far insufficient to provide the required information to understand and predict the behavior of these fluids in practical applications.

Besides the information provided above, it is also important to note that capillary rheometry requires a larger amount of fluid sample than rotational rheometry, slip can often be a problem difficult to determine, and capillary rheometers are much less versatile than rotational ones since neither transient, oscillatory, nor normal stress measurements are possible [15]. Because of all the argued reasons, capillary rheometry does not seem to be the most convenient approach for steady shear flow measurements with STF.

2.2.2 *Transient Shear Flows*

As mentioned before, STF will find practical applications in which its time-dependent behavior is of paramount importance, irrespective of whether it will be used in anti-impact protective equipment or in anti-vibration systems. Moreover, it is known that STF exhibits a much different rheological response when undergoing transient impact experiments than under the steady shear state, as described in the previous section; for instance, DST suspensions support stress orders of magnitude larger under impact conditions than inferred from steady state rheometer measurements [37–39]. Again, these transient results support the idea that any generalized Newtonian fluid model [8, 40–49] will provide information with limited utility from the practical point of view [50]. Thus, a more complete rheological characterization including both the steady state and transient behaviors would be required to provide

theoreticians with useful data sets to develop a constitutive model able to predict time-dependent behaviors such as kinetic models [51].

Transient shear experiments cannot be executed with a capillary rheometer, but by means of rotational rheometers, and, ideally, they should always be performed with a cone-plate geometry, since the shear rate is constant throughout the volume sample. The use of parallel plates is discouraged because the shear strain and stress vary in the radial direction, which is even more inconvenient in transient experiments than in steady shear measurements because it causes a variable shear history throughout the volume sample that complicates the interpretation of the results [15].

In this section, transient experiments are referred to as unsteady shear flows under continuous rotation of the geometry in the rotational rheometer. Oscillatory experiments will be considered as a different group of unsteady shear flow. The variety of transient experiments available in the literature is quite wide [1]; hereafter, the different experiments, the information that they can provide, the precautions that should be considered, and the usefulness for characterizing STF will be considered.

Startup experiments, when applied to STF, should be preferably performed in control-stress mode, for the same reason argued in the previous section. Before the beginning of the experiment ($t < 0$), the fluid sample is at rest; at $t = 0$ constant shear stress is imposed on the fluid: $\tau(t \geq 0) = \tau_0$. This experiment aims at looking at the time evolution of the transient viscosity ($\eta^+(t, \tau_0)$), first normal stress coefficient ($\Psi_1^+(t, \tau_0)$), and second normal stress coefficient ($\Psi_2^+(t, \tau_0)$), which will also depend on the magnitude of the applied shear stress. This sort of experiment allowed Rathee et al. [52] to study localized stress fluctuations in dense suspension, for instance.

Tassieri and his co-workers [53] have developed a Fourier transform-based method (i-Rheo) to determine the viscoelastic moduli from raw startup experimental data in control-stress mode. The efficacy of i-Rheo was validated with colloidal suspensions, both in the fluid and in the glass states [54]; nevertheless, they did not validate it for STF. In this sense, i-Rheo might be an excellent tool for determining the viscoelastic moduli of STF at high frequencies, beyond the limits of rotational rheometers, which are related either to the instrument or to the fluid inertia [3].

From the practical point of view, it may be important to understand how the STF relaxes upon releasing the load [50], how long it will take to be ready for the next load, or even whether it comes to the same initial structure prior to the released load (anti-thixotropy or rheopexy) [55–58]. *Stress relaxation* experiments consist of observing how the shear stress relaxes with time when the flow is abruptly stopped, which allows to determine a relaxation time in shear; this kind of experiment was used by Cho et al. [59] to discover that STF exhibiting DST retains its memory of the level of frictional contacts prior to the flow cessation even after the relaxation ends, despite the presence of the inter-particle repulsions that enable DST.

Concatenated stepwise experiments have been typically used for characterizing thixotropy, but they have been also proven to be useful for characterizing anti-thixotropy or rheopexy (Fig. 2.3). Rubio-Hernández et al. [51] used this experimental protocol to verify that fumed silica suspensions with CST behavior exhibited

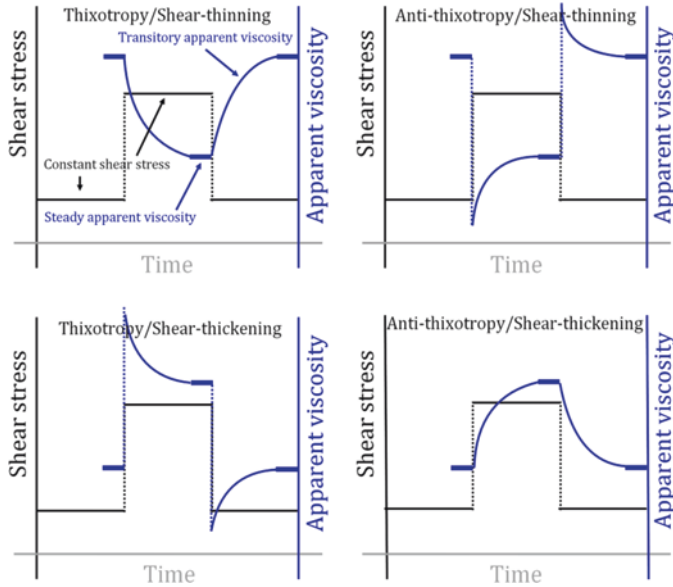


Fig. 2.3 Possible evolution in the apparent viscosity with time in a three-step test applied to shear thinning and shear thickening materials [51]. Reprinted by permission from AIP Publishing

thixotropy within the shear thinning region and anti-thixotropy in the shear thickening region [51].

Hysteresis loops have also been traditionally used to determine thixotropic behavior, although the existence of hysteresis loops is not a synonym of thixotropy; as aforementioned, the existence of thixotropy can only be determined with concatenated stepwise experiments. The hysteresis loop experiment consists of imposing an increasing ramp in shear rate with time followed by a decreasing ramp with the same slope, and register the time evolution of the transient viscosity for each ramp, i.e., $\eta_1^+(t, \dot{\gamma}_1)$ for the increasing ramp with slope $\dot{\gamma}_1$ and $\eta_2^+(t, \dot{\gamma}_2)$ for the decreasing ramp with slope $\dot{\gamma}_2 = -\dot{\gamma}_1$. Results are typically represented as η^+ vs $\dot{\gamma}$, and if the curves given by η_1^+ and η_2^+ do not overlap, it is said that there is a hysteresis loop; nevertheless, they can also be found in terms of stress versus shear rate (Fig. 2.4).

In STF, if the first and second ramps lie within the limit of the shear thinning region ($\dot{\gamma} < \dot{\gamma}_c$), then the presence of a hysteresis loop would mean that there is a difference between the kinematics of the destruction of the microstructure during the increasing ramp and the kinematics of construction of the microstructure during the decreasing ramp; if the first and second ramps go within the limits of the shear thickening region ($\dot{\gamma}_c < \dot{\gamma} < \dot{\gamma}_{max}$), then the kinematics of construction of the shear-induced microstructure during the increasing ramp is different from the kinematics of destruction of the microstructure dominated by repulsive forces during the decreasing ramp. If the experiment provides overlapping curves, then it would mean

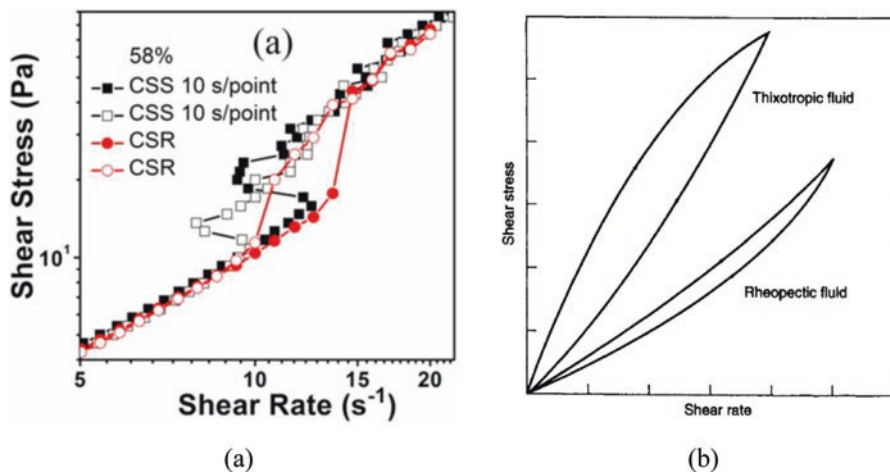


Fig. 2.4 (a) Up and down flow curves displaying hysteresis of shear thickening suspensions. Filled symbols for increasing stress and open symbols for decreasing stress sweeps [60]. Reprinted by permission from American Physical Society. (b) Schematic shear-stress rate behavior for time-dependent fluid behavior [61]. Reprinted by permission from Elsevier

that both kinematics responsible for building and destroying microstructure are essentially equal. It is recommendable to test different slopes as in [62].

Flow reversal tests consist of imposing a shearing flow in one direction and instantaneously changing the direction of the flow while the magnitude of the shear rate remains the same [63]. This kind of test has been traditionally used to validate constitutive models for thixotropic fluids, which typically exhibit a two-step relaxation of shear stress caused by the presence of a viscoelastic relaxation and a kinematic hardening relaxation [58]. Nevertheless, there is no fundamental reason for not using the flow reversal tests in validating kinematic models for time-dependent behavior of STF; however, to the best of the author's knowledge, the state of the art lacks this experimental data sets.

It can be found in the literature that unsteady shear flow tests are typically complemented with simultaneous confocal microscopy [64], boundary stress microscopy [65] X-ray [66] pressure measurements [67], or ultrasound imaging [68] in order to provide extra information regarding the presence or the evolution of microstructures, heterogeneities, vortices bands, etc., developed in the fluid sample along the experiment.

2.2.3 Oscillatory Shear Flows

Oscillatory shear flow experiments allow to decouple the viscoelastic response of a complex fluid into the elastic contribution and the viscous contribution; these viscous and elastic forces lead to an additional time scale and help to provide more

insight into a controllable alternative shear history in comparison to steady shear experiments [69].

Typically, a sinusoidal shear stress or strain is imposed, and the resulting strain or stress is recorded; therefore, the material functions (G' and G'') are defined with the output signal. This way, when a sinusoidal strain signal is applied, the stress wave that is in phase with the applied strain wave divided by the amplitude of the strain wave is called the *storage modulus* (G'). On the other way, the amplitude of the stress wave that is out of phase with the strain wave divided by the strain amplitude is called *loss modulus* (G''). If the sample is a Hookean solid, both signals are in phase ($G'' = 0$); in the case of a Newtonian liquid, the signals are shifted by $\frac{\pi}{2}$ ($G' = 0$), and in the case of a viscoelastic liquid, the signals are shifted by a phase angle $0 < \delta < \frac{\pi}{2}$ (G' and $G'' \neq 0$) as illustrated in Fig. 2.5.

The first step to analyze a sample by means of an oscillatory test is to perform an amplitude sweep. This test consists in applying a strain or stress amplitude sweep at a constant frequency and the typical results are represented in Fig. 2.6. These results allow one to determine the limit of the linear viscoelastic region (LVR), in which the viscoelastic moduli do not vary with the strain amplitude indicating that the structure is still preserved.

The frequency sweep test must then be developed by choosing a strain within the LVR. The frequency sweep test gives information on the time-dependent behavior of the sample in a non-destructive interval of strain/stress and consists in applying a

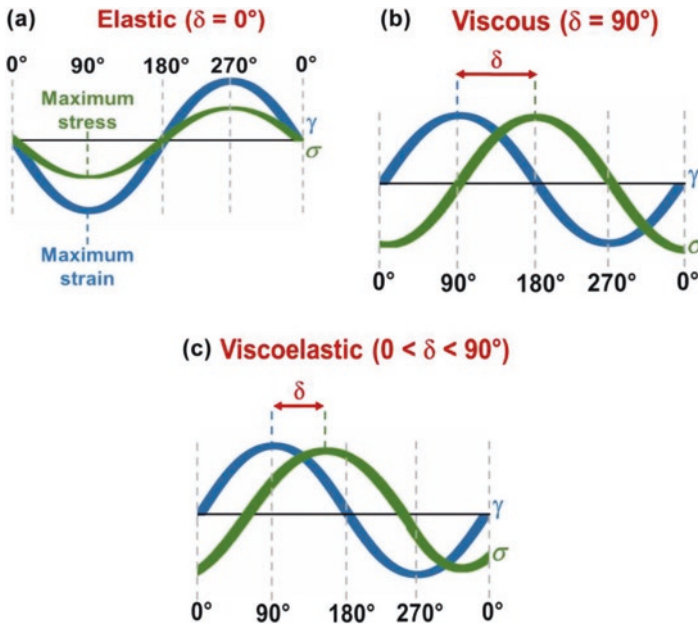


Fig. 2.5 Stress and strain wave relationships for (a) a purely elastic (ideal solid), (b) a purely viscous (ideal liquid), and (c) a viscoelastic material [70]. Under the Creative Commons license

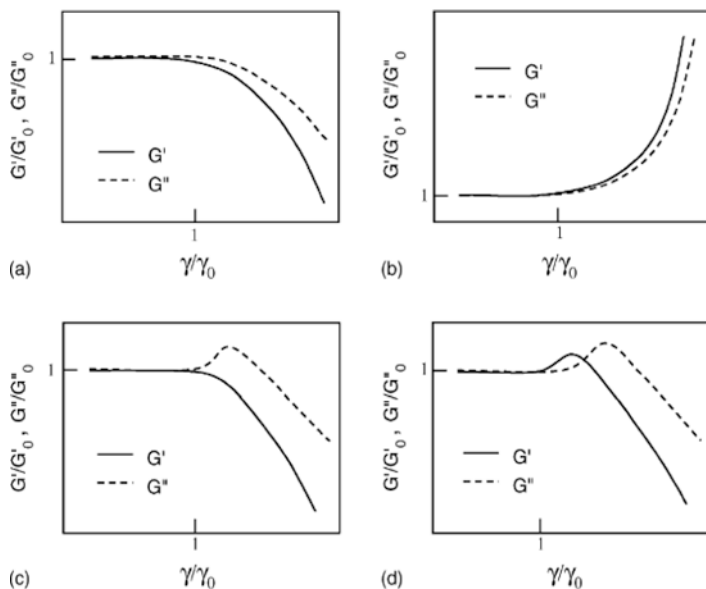


Fig. 2.6 Types of LAOS behavior: (a) strain thinning, (b) strain hardening, (c) weak strain overshoot, (d) strong strain overshoot [71]. Reprinted by permission from Elsevier

frequency sweep at a constant strain from the LVR. However, the complex behavior of STF is not observed in this kind of experiment because of the small magnitude of the applied strain. Under certain conditions (high deformation, high volume fraction, high frequency, etc.), the signal response is no longer sinusoidal indicating the limit of the LVR and more harmonics appear that can give valuable information about the microstructure of the sample. Experimental tests performed in this region are called large oscillatory shear tests (LAOS) as opposed to their counterparts developed at low deformations, small amplitude oscillatory tests (SAOS). Several studies have been carried out during decades to understand the dynamic behavior of STF using oscillatory tests: e.g., Laun et al. [72], Boersma et al. [73], Raghavan and Khan [74], Yziquel et al. [75], Mewis and Biebaut [69], Lee and Wagner [76], Fischer et al. [77], Chang et al. [78], Khandavalli and Rothstein [79], Lee et al. [80], Rathee et al. [65].

Hyun et al. [71] wrote about the importance of LAOS experiments to characterize complex fluids such as STF. They basically classified the complex fluids into four types: type I, with G' and G'' decreasing (strain thinning); type II, with G' and G'' increasing (strain hardening); type III, with G' decreasing and G'' increasing followed by a decrease (weak strain overshoot); and type IV, with both G' and G'' increasing followed by a decrease (strong strain overshoot). Figure 2.6 is a schematic representation of these types of LAOS behaviors. Typically type IV is very representative of STF as is shown in Raghavan and Khan [74] and Galindo-Rosales et al. [18], for example.

Boersma et al. [73] studied the nonlinear viscoelastic behavior of dispersions of silica (SiO_2) particles in a glycerol/water mixture and dispersions of glass particles in a glycerol/water mixture. They found that G'' dominates over G' , indicating a liquid-like behavior because of the absence of flocculation. A nonlinear response was observed after a critical combination of frequency and deformation. When larger strain amplitudes and frequencies are applied to STF, the viscoelastic modulus increases abruptly (strain hardening). Raghavan and Khan [74] analyzed the rheological behavior under oscillatory tests of suspensions of fumed silica in polypropylene glycol. They reported strain hardening behavior and demonstrated that this behavior at high strain amplitudes is quite similar to shear thickening in steady flow experiments. This correlation can be represented using a modified Cox-Merz rule (proposed by Doraiswamy et al. [81]) in which the results of the complex viscosity as a function of dynamic shear rate ($\dot{\gamma}_0 \cdot \omega$) can be superposed with the results of the viscosity in steady shear experiments. Also, three different fumed silica particles suspended in polypropylene glycol and in paraffin oil were used by Yzique et al. [75] to analyze the linear and nonlinear rheological behavior. They observed solid-like behavior ($G' > G''$) for the three different silica particles at 8.2 wt% in paraffin oil. It was not possible to observe the linear regime as the loss modulus increased with the strain amplitude at low values of strain, possibly due to the breakdown of the structure. On the contrary, for the suspension in polypropylene glycol, the loss modulus was higher than the elastic modulus, indicating a liquid-like behavior. In the nonlinear regime, they observed excess dissipation energy (calculated from amplitudes sweeps) because of the breakdown of the 3D structure of the fumed silica suspensions. Mewis and Biebaut [69] observed also a strain hardening in oscillatory flow for monodispersed silica core particles with a grafter layer of poly(butyl methacrylate) (PBMA) in octanol. They found that the critical stress at which the strain hardening occurs is independent of the frequency and is also the same as the critical shear stress in steady flow measurement when the shear thickening appears. They also concluded that for their systems, the onset for the strain hardening is independent of the flow history, since in the oscillatory flow, the critical conditions are obtained periodically and lead to the same effect as reaching the critical conditions in continuous regime. Lee and Wagner [76] investigated the critical strain amplitude able to provoke shear thickening in oscillatory flow and the frequency dependence. They showed that neither the extent nor the modified Cox-Merz rules were able to correlate the dynamic and the steady state viscosities in the shear thickening regime or in the onset of the shear thickening. They proposed a superposition of the two viscosities at the point when the shear thickening regime can be observed by plotting the data versus the average stress magnitude. For low frequencies, the critical strain varies inversely with the frequency, but for high frequencies, an apparent plateau appears because of a large amount of slip. Fischer et al. [77] used in their studies concentrated suspensions of hydrophilic fumed silica in polypropylene glycol. They performed frequency sweep experiments for a wide range of strain amplitudes and found a power law correlation showing a decrease in the viscosity with frequency before and after the transition, being the effect more marked at frequencies after the transitions, leading to think that the shear thickening

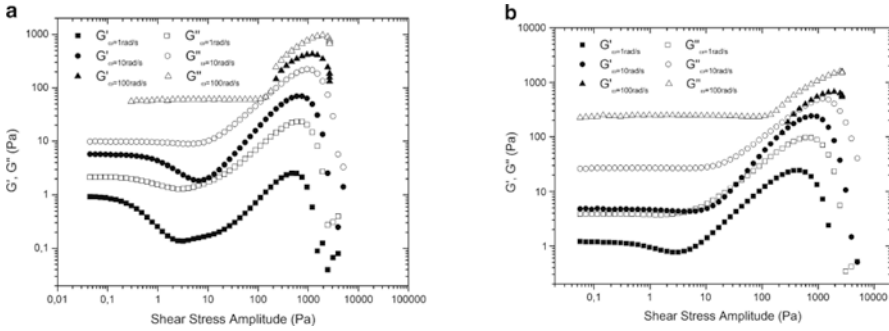


Fig. 2.7 Amplitude sweeps of Aerosil R816 suspensions in (a) PPG400, (b) PPG2000 [18]. Reprinted by permission from Springer

could disappear at sufficiently high frequencies. Galindo-Rosales et al. [18] used hydrophobic fumed silica in polypropylene glycol. Fig. 2.7 shows the results of the amplitude sweep tests: the loss modulus (G'') is higher than the elastic modulus (G'), typical of a liquid-like behavior, but both moduli present relatively low values according to the non-flocculated nature of the suspensions. As it was reported previously, at a certain value of the stress amplitude, both moduli increase abruptly revealing the strain hardening behavior.

A deep-inside analysis of the LAOS experiments was developed by Khandavalli and Rothstein [79]; they evaluated the rheological properties of three different suspensions—fumed silica in polyethylene oxide, fumed silica in polypropylene glycol, and cornstarch in water—and found a type III and type II LAOS behaviors for G' and G'' for the fumed silica in polyethylene oxide and in polypropylene glycol respectively (according to the classification of Hyun et al. [71]). For the cornstarch in water suspension, the results were $G' \geq G''$, and as the strain amplitude increased, the moduli declined, but at large strain amplitudes, G' and G'' increased showing a strain-rate thickening behavior. The Lissajous-Bowditch curves were useful to analyze the viscoelastic nonlinearities which revealed strong differences between the samples. Rathee et al. [65] also analyzed the LAOS response of colloidal suspensions formulated with silica particles in a glycerol/water mixture in a regime of discontinuous shear thickening, obtaining results consistent with the ones of Khandavalli and Rothstein [79].

The analysis of the viscoelastic properties in the nonlinear regime by means of LAOS experiments is of great importance for the development of damping materials and their applications to energy absorption and vibration control. The analysis of the energy dissipation capacity of a damper is normally done through a hysteresis curve in which the enclosed area is the consumed energy of the structure in one cycle, similarly to the Lissajous-Bowditch curves obtained in LAOS experiments. Some work related to the development of optimized dampers aimed to develop dynamic models for dampers with STF (Zhao et al. [82], Zhang et al. [83], Lin et al.

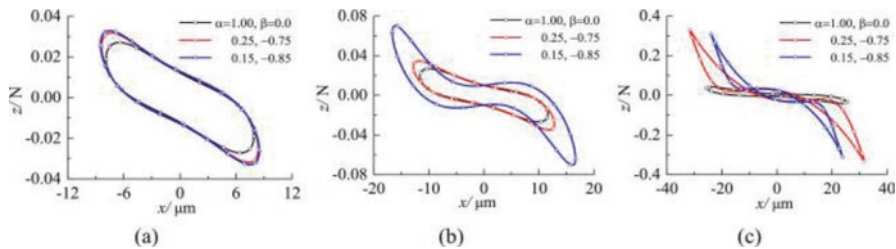


Fig. 2.8 Hysteric curves with different excitation frequency and amplitude: (a) $f = 35$ Hz, $F = 2$ N, (b) $f = 50$ Hz, $F = 2$ N, (c) $f = 50$ Hz, $F = 5$ N [85]. Reprinted by permission from Elsevier

[84], Zhao et al. [85]). The hysteric curves with different excitation frequency and amplitude developed by Zhao et al. [85] are shown in Fig. 2.8 and can be easily compared with the data from LAOS.

2.2.4 Superposition Rheology

Superposition in rheology means that during the experiment, both steady shear deformation and oscillatory motion are simultaneously applied to the sample. The directions of the velocity vectors of each motion can be either parallel, thus designating a parallel superposition, or at right angles, known as transverse or orthogonal superposition. The parallel shear stress superposition is represented in Fig. 2.9 and given by $\tau_{yx}(\dot{\gamma}, \gamma_0, t) = \eta(\dot{\gamma}) \cdot \dot{\gamma} + G_{\parallel}^* (\omega, \dot{\gamma}, \gamma_0) \cdot \gamma_0 \cdot \sin(\omega \cdot t)$, where G_{\parallel}^* is the parallel complex modulus, $\dot{\gamma}$ is the steady shear rate, $\eta(\dot{\gamma})$ is the steady shear viscosity, and γ_0 and ω are the amplitude and frequency of the superimposed oscillation, respectively [87, 88].

Although data interpretation regarding superposition rheology is still under investigation since the viscoelastic superposition response on a microscopic level is rather complex, the technique is very powerful as it provides valuable information regarding the material's viscoelasticity under nonlinear perturbation [89]. The effects of parallel superposition have been gradually investigated in shear thickening suspensions, such as in the work of Mewis and Biebaut [69] where suspensions of silica particles in poly(butyl methacrylate) (PBMA) were subjected to parallel superposition eliminating or reducing the contributions from the longest relaxation times during the experiments and evidencing shear thickening behavior before the steady state viscosities start to increase. Recently, Rubio-Hernández [86] tested a concentrated fumed silica suspension in polypropylene glycol (PPG) with parallel superposition rheology. They concluded that, for simple oscillatory measurements, the loss modulus dominated $G'' > G'$, contrary to what happened with superimposed testing, where $G' > G''$, suggesting that the microstructure of the STF evolved from few and big hydroclusters on the onset of the shear thickening region to many and small ones when shearing increases.

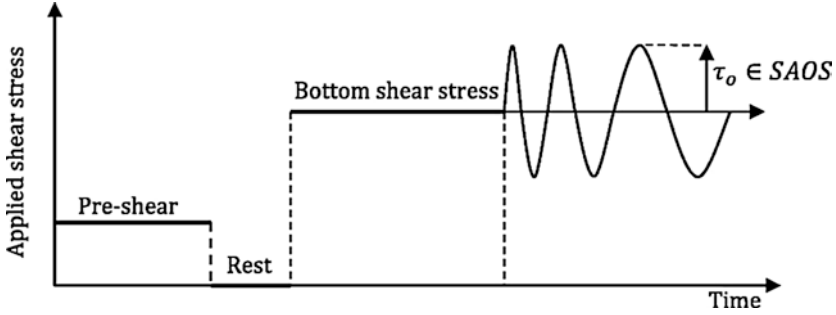


Fig. 2.9 Parallel superposition (steady shear rate and SAOS) protocol [86]. Reprinted by permission from Elsevier

2.3 Extensional Rheometry of STF

Even though most of the real flow conditions are complex—i.e., they consist of a combination of shear, rotation, and extensional flows, and it has become evident that just by shear rheometry, it is not possible to properly model the behavior of complex fluids—the truth is that extensional rheometry is underdeveloped when compared to shear rheometry. The reason is that imposing a surface-free uniaxial extensional flow is challenging, particularly for mobile liquids, such as suspensions or polymeric solutions. Only the Filament Stretching Extensional Rheometer (FiSER™) and the Capillary Breakup Extensional Rheometer (CaBER®) have given proof of merits for rheometric purposes. Both devices are based on the filament stretching approach, but whereas the FiSER™ imposes a constant extension rate, the CaBER® device imposes a step-strain deformation out of the equilibrium and the filament thinning process is performed under capillary forces and at an uncontrolled extension rate. In any case, they are both considered accurate methods for characterizing viscoelastic polymeric solutions, particularly when operated with simultaneous high-speed imaging [5]; nevertheless, in recent years, their use has been extended to other complex fluids such as emulsions [90, 91] or suspensions [25, 92–97]. The extensional properties of STF have also been characterized with success by means of the FiSER™ [25, 49, 98–100] and the CaBER® [25, 101, 102] devices in the recent years.

In both devices, the initial aspect ratio $\left(\Lambda_0 = \frac{h_0}{d_0}\right)$ introduces an important shear component in the flow at the early stages of the experiment. In order to minimize the shear effects, the FiSER™ device can impose two steps in the stretching protocol: in the first step, the liquid bridge is stretched at a small extension rate, well below the onset of extensional thickening and when the aspect ratio is large enough, ideally $\frac{1}{\Lambda_0^4} \sim 0$; and in the second step, the desired extension rate ($\dot{\epsilon}$) is imposed [25]. Further investigations about the influence of systematically introducing a controlled pre-deformation history can be found in [103]. The force sensors provide information about the time evolution of the pulling force exerted by the liquid on the

plates, $F(t)$, and then the tensile stress difference generated within the filament can be calculated: $\tau_{zz} - \tau_{rr} = \frac{4F(t)}{\pi d_{\min}^2(t)} + \frac{1}{2} \frac{\rho g \pi h_0 d_0^2}{4\pi d_{\min}^2(t)} - \frac{2\sigma}{d_{\min}(t)}$. Thus, the transient

extensional viscosity is given by $\eta_E^+(t) = \frac{\tau_{zz} - \tau_{rr}}{\dot{\epsilon}}$. Although CaBER[®] can provide

interesting information about the extensional rheometry of STFs, it possesses three significant drawbacks: (i) it cannot perform the two-step stretching protocol and, therefore, the experimentalist must take that into account for the analysis of the results; (ii) it can only control the initial extension rate until reaching the final separation, upon when the filament thinning process undergoes an uncontrolled extension rate, which has to be calculated from the time evolution of the minimum

diameter as $\dot{\epsilon} = \frac{-2}{d_{\min}(t)} \frac{d(d_{\min}(t))}{dt}$; (iii) CaBER[®] is not originally equipped with a

force transducer, thus the extensional viscosity can only be estimated by means of surface tension and the time evolution of the filament radius $\left(\eta_E^+ \approx \frac{-\sigma}{d(d_{\min}(t))/dt} \right)$.

Temperature control in the FiSER[™] and CaBER[®] is not as good as in the rotational rheometers, where the bottom plate geometry is typically equipped with a Peltier temperature controller. Thus, if it is intended to work at a different temperature, it is recommended to have the sample in an external bath at the required temperature and quickly load the sample and run the experiments, which are very fast and temperature evolution could be neglected.

2.4 Field-Responsive STF

In magnetorheology [104] and electrorheology [105], an external magnetic and electric field is imposed, respectively, to the fluid sample while the rheological experiment is undergone. For this purpose, commercial rotational rheometers can be equipped with a magnetorheological cell or an electrorheological cell and, in both cases, the external field imposed is steady and perpendicular to the direction of the flow field. The presence of either the electric field or the magnetic field induces a microstructure of particles aligned in the direction of the field, which typically results in an increase of the yield stress. Very recently, M. Terkel and J. de Vicente have developed a new magnetorheological cell able to impose unsteady and triaxial magnetic fields [106, 107]. Consequently, exotic magnetic mesostructures can be generated, resulting in an enrichment of the magnetorheological response. Nevertheless, this degree of freedom in terms of control of the direction and unsteadiness of the electric field has not been reached yet for the electrorheological cells of the rotational rheometers.

Regarding the extensional rheometry, researchers from the Transport Phenomena Research Center [108] have recently developed a series of magnetorheological [92,

Table 2.2 Possible field flow configurations currently available in - and electrorheometry

Field	Configuration	Shear flow	Extensional flow
Magnetic	Parallel	Possible	Possible
	Perpendicular	Possible	Possible
Electric	Parallel	Not possible	Possible
	Perpendicular	Possible	Not possible

[94] and electrorheological [94] cells able to impose steady and uniaxial external magnetic fields and electric fields, respectively, to the fluid sample when characterized under extensional flow in the CaBER® device. In the case of extensional magnetorheometry, two add-ons were designed allowing to choose the direction of the magnetic field either parallel or perpendicular to the extensional flow, whereas in the case of extensional electrorheometry, only one add-on was created and the electric field can only be imposed aligned with the direction of the flow. Table 2.2 summarizes the current state of the art in terms of possible configurations to perform magneto- and electrorheological measurements.

Despite the magnetorheological effect being traditionally linked to an increase in viscosity and yield stress under shear flow operating in the perpendicular configuration, it is possible to formulate magnetorheological STF (MRSTF) by dispersing carbonyl iron particles in a carrier fluid exhibiting shear thickening behavior [109–113], allowing to control the shear thickening behavior with the presence of the external magnetic field. Very recently, Bossis et al. [114] reported an outstanding magnetorheological effect based on discontinuous shear thickening. Their MRSTF was formulated by dispersing carbonyl iron particles in water using a superplasticizer molecule, which allowed to reach a volume fraction as high as 62% with a small yield stress and a still low plastic viscosity. The DST behavior is the consequence of particle-particle friction [115]. In their rheological characterization, they used parallel plates with serrated surfaces to avoid slip, and the results showed that by increasing the intensity of the magnetic field, the jamming transition occurred at smaller shear rates. Because the torque range in the rotational rheometer is too low for this kind of samples and because the radial stress developed during the jamming expels the particles from the suspension, they designed a viscometer able to hold ten times larger torques and based on a double helix geometry, which behaves approximately as a cylinder and avoids sedimentation, thanks to the induced small flow along the axis; the outer cylinder had vertical stripes to prevent wall slip.

In the electrorheological effect, the presence of an external electric field also results in an increase in the viscosity and yield stress under shear flow operating in the perpendicular configuration. Nevertheless, the application of an external electric field is also able to affect the shear thickening behavior of certain suspensions. That is the case of the E-FiRST (Electric Field Responsive Shear Thickening), which was first reported by Shenoy et al. [116]; instead of enlarging the shear thickening response of the fluid, in the E-FiRST effect, the presence of an external field allows to suppress the onset of shear thickening and, subsequently, the resistance to flow at high shear rates. In that study, non-serrated plates were used in a strain-controlled

rheometer. Tian and co-workers [117, 118] reported a reversible shear thickening of electrorheological fluids above a low critical shear rate and a high critical electric field strength; their fluid sample consisted of a dispersion of NaY zeolite particles coated with glycerin in silicone oil, which was tested in a two concentric cylinder geometry by means of shear rate ramp tests.

2.5 Non-conventional Rheometry of STF

Apart from the latest works on the application of STF for polishing optical components and vibration control [119, 120], most of the vast research related to STF is dedicated to protective applications [6], such as the development of anti-impacts [121–125], anti-blast [126–128], bullet proof [129, 130], or stab/spike-resistant [131–135] materials.

In these impact protection applications, STF undergoes either low or high velocity impacts, which impose a flow to the liquid that is intrinsically transitory and, therefore, obviously far from the experimental conditions imposed in the rotational rheometer leading to the steady state viscosity/flow curves. Moreover, even if the rheologist wanted to measure the “instantaneous” flow curve in the rheometer, that curve would only be reliable if the time between points would be over 15 ms, because of the instrument and fluid’s inertias [14]. In low-velocity impact tests, the characteristic timescale for the composite providing the maximum force in its response is smaller than 5 ms, which will be much shorter in the case of bullet proof, stab/spike-resistant, or anti-blast applications. So, there is no doubt that new experimental approaches are required to provide the determination of the time-resolved viscosity curve of a liquid sample with a time resolution of the order of milliseconds at most.

Sliding plate rheometers [136–138] have proven to be an alternative to rotational rheometers for the characterization of shear thinning fluids under “large, rapid, transient shear deformations”, allowing the measurement of normal stresses [139] and reaching high frequencies when reducing the gap size down to the microscale [140–142]. This latter feature, characterizing STF at frequencies in the order of 10 kHz, is of paramount importance because, on the one hand, it enables a fine analysis of the interplay between local scale hydrodynamics and inter-particle forces [143], and that information can help in the development of new formulations of STF; on the other hand, it allows developing fluid models that can be used in practical dampers’ design for motion stages [144]. Sliding cylinder rheometers are similar to sliding plate rheometers, but they prevent edge effects and bearing friction issues. The principle of the sliding cylinder rheometer is also similar to the principle of the falling rod viscometer, which is considered a precise method for measuring the absolute viscosity of Newtonian fluids ranging from 10 to 10^7 Pa·s [145, 146]. In these three kinds of rheometers, when the relative gap between the plates or cylinders is very small, there is no need to know the constitutive equation of the fluid to calculate the shear strain and shear rate, as in the rotational rheometer. Although they have proven

to be useful for highly viscous systems, such as polymer melts [147] and others [144, 145], to the best of the authors' knowledge, it has not been reported in the literature their performance when dealing with STF.

Bikerman's penetrometer [146] for determining the viscosity of Newtonian fluids under steady state conditions is able to provide viscosity measurements between 10^2 and 10^5 Pa·s with an error below 3.5%. As in the falling rod viscometer, the fluid sample is contained between two coaxial cylinders in which the inner one moves downward and the outer is fixed; however, unlike the falling rod rheometer, the area of contact does not remain constant in the penetrometer and the fluid is forced to flow upward through the annular gap between the two cylinders. This kind of flow is currently known as back extrusion flow or annular pumping flow, which is the basis of the back extrusion technique (BET) [148], which is mainly used in food engineering [149–152] to evaluate the rheological properties of the power-law or Herschel-Bulkley fluids in general, but it can also be used for determining the viscoelastic moduli of concentrated polymer solutions by imposing an axially oscillatory movement with a very small amplitude to the inner cylinder [153]. Based on the BET, Hoshino [154–156] has recently developed the Short Back Extrusion (SBE) method, which is able to provide good agreement with the steady viscosity curves measured with a rotational rheometer; however, SBE is not suited for high speed measurements. Fakhari and Galindo-Rosales [14] analyzed the possibility of measuring transient shear viscosity at large, rapid, and transient shear deformation by imposing a back extrusion flow; an analytical expression for the instantaneous viscosity relating the friction force at the inner cylinder wall to its velocity by means of a geometric factor was validated providing an accuracy of ~93% for Newtonian fluids and for the right set of parameters in the experiment within a timescale of the order of ~2 ms; however, it has not been validated yet for STF, neither analytically, numerically, nor experimentally.

The split-Hopkinson pressure bar (SHPB) is typically used for the characterization of dynamic mechanical properties of materials and it has also been used for characterizing STF in transient squeeze flows at high compression rates, which are characteristics of an impact event [157–160]. It consists of a gas gun and three cylindrical bars, i.e., a striker bar, an incident bar, and a transmission bar; during the experiment, the incident wave, the reflection wave, and the transmission wave are recorded by means of strain gauges (Fig. 2.10). Lim et al. [162] discussed in detail the conditions under which classic SHPB data analysis is applicable for Newtonian fluid samples and they found a good agreement between the theory and the experiment obtained for thin specimens (~1 mm) across a wide range of shear strain rates (over 10^5 s⁻¹). Despite this technique providing useful information for the development of STF to be used under high-velocity impact applications, further work is still required for determining the material properties from the SHPB measurements, as it was done previously for Newtonian fluids [162]. For STF, this would require a robust constitutive model and/or independent measurements of the kinematics in the sample during deformation [157].

Very recently, Madsen et al. [163] developed a non-intrusive technique able to provide instantaneous viscosity up to a timescale on the order of 20 μ s. They

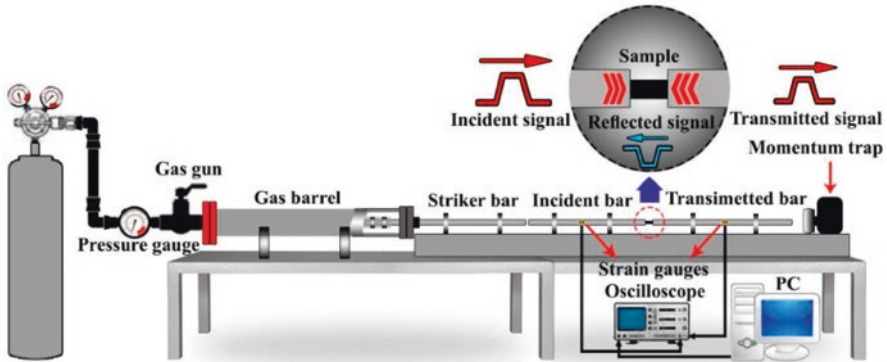


Fig. 2.10 Schematics of the split-Hopkinson pressure bar (SHPB) [161]. Under the Creative Commons license

developed a structured-light detection system that allows particle tracking over femtometer length scales and 16 ns timescales, which allows the determination of the instantaneous velocity of a trapped particle in an optical tweezer. In the ballistic regime, where the measurement is fast compared to the particle's momentum relaxation time, the viscosity can be obtained more directly through its connection to kinetic energy dissipation. Neglecting hydrodynamic memory effects, collisions with molecules in the fluid exponentially damp the velocity of the particle over the momentum relaxation time. This momentum relaxation typically occurs at a much faster rate than the position relaxation, which allows for reducing the integration time required for precise viscosity measurements and, therefore, increases the speed of the measurement. The method was only validated for Newtonian fluids with viscosities ranging from 0.3 to 1.9 mPa·s with temporal resolution between 20 μ s and 1 ms; therefore, further research would be required to validate it for STF.

2.6 Future Perspectives

In the last decade, STF has proven to be very popular in protective applications [6]. Most of the published work aims the application of STF in fabric development for body protection technology. The range of STF application is quite extensive. There are several works in the literature regarding sports products (athletic rackets), medical products (surgical gloves or gowns), space technology, electronics and sensing, or even the petrochemical industry [164].

Rheology is a powerful tool that has been only exploited to its most in the characterization of STF when scientists tried to unveil the physics behind this fluid. The use of rheology has been typically limited to providing just their viscosity curves. It is essential to understand that STF will undergo transient and complex flows in real applications, and viscosity curves will fall short in predicting their response. Therefore, a complete rheological characterization can better predict how STF will perform in real flow conditions.

It becomes evident that to better predict the fluid-flow features of STF under real conditions allowing the development of new composites, it is of paramount importance to develop new and more realistic constitutive models for STF that goes beyond the current generalized Newtonian fluid models. These new constitutive models should be able to predict the viscoelastic nature based on the experimental information that a complete rheological characterization is able to provide. This is a challenge for the rheology community in the years to come.

Acknowledgments Authors would like to acknowledge the financial support from FEDER funds through COMPETE2020-Programa Operacional Competitividade e Internacionalização (POCI) and FCT/MCTES LA/P/0045/2020 (ALiCE), UIDB/00532/2020, UIDP/00532/2020 (CEFT), and UI/BD/150887/2021, funded by national funds through FCT/MCTES (PIDDAC) and NORTE-01-0145-FEDER-000054.

References

1. F.A. Morrison, A.P.C.E.F.A. Morrison, *Understanding Rheology* (Oxford University Press, 2001) <https://books.google.pt/books?id=bwTn8ZbR0C4C>
2. F.J. Galindo-Rosales, Complex fluids and Rheometry in microfluidics, in *Complex Fluid-Flows in Microfluidics*, ed. by F.J. Galindo-Rosales, (Springer International Publishing, Cham, 2018), pp. 1–23
3. R. Ewoldt, M. Johnston, *Caretta L* (How to Avoid Bad Data, Experimental Challenges of Shear Rheology, 2015), pp. 207–241
4. Official symbols and nomenclature of the Society of Rheology. *J. Rheol.* **57**(4), 1047–1055 (2013). <https://doi.org/10.1122/1.4811184>
5. F.J. Galindo-Rosales, M.A. Alves, M.S.N. Oliveira, Microdevices for extensional rheometry of low viscosity elastic liquids: A review. *Microfluid. Nanofluid.* **14**(1), 1–19 (2013). <https://doi.org/10.1007/s10404-012-1028-1>
6. S. Gürgen, M.C. Kuşhan, W. Li, Shear thickening fluids in protective applications: A review. *Prog. Polym. Sci.* **75**, 48–72 (2017) <https://www.sciencedirect.com/science/article/pii/S0079670017300035>
7. E. Brown, H.M. Jaeger, Shear thickening in concentrated suspensions: Phenomenology, mechanisms and relations to jamming. *Rep. Prog. Phys.* **77**(4), 046602 (2014). <https://doi.org/10.1088/0034-4885/77/4/046602>
8. F.J. Galindo-Rosales, F.J. Rubio-Hernández, A. Sevilla, An apparent viscosity function for shear thickening fluids. *J. Non-Newtonian Fluid Mech.* **166**(5), 321–325 (2011) <https://www.sciencedirect.com/science/article/pii/S0377025711000024>
9. E. Brown, H.M. Jaeger, Through thick and thin. *Science* **333**(6047), 1230–1231 (2011). <https://doi.org/10.1126/science.1211155>
10. H.A. Barnes, Shear-thickening (“Dilatancy”) in suspensions of nonaggregating solid particles dispersed in Newtonian liquids. *J. Rheol.* **33**(2), 329–366 (1989). <https://doi.org/10.1122/1.550017>
11. N.J. Wagner, J.F. Brady, Shear thickening in colloidal dispersions. *Phys. Today* **62**(10), 27–32 (2009) <https://www.scopus.com/inward/record.uri?eid=2-s2.0-70349779635&doi=10.1063%2f1.3248476&partnerID=40&md5=96a696a15746a2d14f974ec019d87f7c>
12. T.G. Mezger, C. Sprinz, A. Green, *Applied Rheology: With Joe Flow on Rheology Road* (Anton Paar, 2018) <https://books.google.pt/books?id=xmgBjwEACAAJ>
13. F.J. Galindo-Rosales, Complex fluids in energy dissipating systems. *Appl. Sci.* **6**(8), 206 (2016)

14. A. Fakhari, F.J. Galindo-Rosales, Parametric analysis of the transient back extrusion flow to determine instantaneous viscosity. *Phys. Fluids* **33**(3), 033602 (2021). <https://doi.org/10.1063/5.0033560>
15. J. Mewis, N.J. Wagner, *Colloidal Suspension Rheology* (Cambridge University Press, Cambridge, 2011) <https://www.cambridge.org/core/books/colloidal-suspension-rheology/E4C1D16944B043534881158BC62D3E59>
16. G. Bossis, Y. Grasselli, O. Volkova, Capillary flow of a suspension in the presence of discontinuous shear thickening. *Rheol. Acta* **61**(1), 1–12 (2022). <https://doi.org/10.1007/s00397-021-01305-0>
17. A. Fall, A. Lemaître, F. Bertrand, D. Bonn, G. Ovarlez, Shear thickening and migration in granular suspensions. *Phys. Rev. Lett.* **105**(26), 268303 (2010). <https://doi.org/10.1103/PhysRevLett.105.268303>
18. F. Galindo-Rosales, F. Rubio-Hernández, J. Velázquez-Navarro, Shear-thickening behavior of Aerosil® R816 nanoparticles suspensions in polar organic liquids. *Rheol. Acta* **48**, 699–708 (2009). <https://doi.org/10.1007/s00397-009-0367-7>
19. Y. Madraki, S. Hormozi, G. Ovarlez, É. Guazzelli, O. Pouliquen, Enhancing shear thickening. *Phys. Rev. Fluids* **2**(3), 033301 (2017). <https://doi.org/10.1103/PhysRevFluids.2.033301>
20. A. Fall, N. Huang, F. Bertrand, G. Ovarlez, D. Bonn, Shear thickening of Cornstarch suspensions as a Reentrant jamming transition. *Phys. Rev. Lett.* **100**(1), 018301 (2008). <https://doi.org/10.1103/PhysRevLett.100.018301>
21. J.M. Dealy, J. Wang, Viscosity and normal stress differences, in *Melt Rheology and its Applications in the Plastics Industry*, ed. by J.M. Dealy, J. Wang, (Springer Netherlands, Dordrecht, 2013), pp. 19–47
22. C.D. Cwalina, N.J. Wagner, Material properties of the shear-thickened state in concentrated near hard-sphere colloidal dispersions. *J. Rheol.* **58**(4), 949–967 (2014). <https://doi.org/10.1122/1.4876935>
23. C.W. Macosko, *Rheology: Principles, Measurements, and Applications* (VCH, New York, NY, 1994)
24. H.M. Laun, Normal stresses in extremely shear thickening polymer dispersions. *J. Non-Newtonian Fluid Mech.* **54**, 87–108 (1994) <https://www.sciencedirect.com/science/article/pii/0377025794800162>
25. R.J.E. Andrade, A.R. Jacob, F.J. Galindo-Rosales, L. Campo-Deaño, Q. Huang, O. Hassager, et al., Dilatancy in dense suspensions of model hard-sphere-like colloids under shear and extensional flow. *J. Rheol.* **64**(5), 1179–1196 (2020). <https://doi.org/10.1122/1.5143653>
26. Z. Pan, H. de Cagny, M. Habibi, D. Bonn, Normal stresses in shear thickening granular suspensions. *Soft Matter* **13**(20), 3734–3740 (2017). <https://doi.org/10.1039/C7SM00167C>
27. O. Maklad, R.J. Poole, A review of the second normal-stress difference; its importance in various flows, measurement techniques, results for various complex fluids and theoretical predictions. *J. Non-Newtonian Fluid Mech.* **292**, 104522 (2021) <https://www.sciencedirect.com/science/article/pii/S0377025721000458>
28. J.F. Morris, Shear thickening of concentrated suspensions: Recent developments and relation to other phenomena. *Annu. Rev. Fluid Mech.* **52**(1), 121–144 (2020). <https://doi.org/10.1146/annurev-fluid-010816-060128>
29. E. Brown, H.M. Jaeger, The role of dilation and confining stresses in shear thickening of dense suspensions. *J. Rheol.* **56**(4), 875–923 (2012). <https://doi.org/10.1122/1.4709423>
30. S. Garland, G. Gauthier, J. Martin, J.F. Morris, Normal stress measurements in sheared non-Brownian suspensions. *J. Rheol.* **57**(1), 71–88 (2012). <https://doi.org/10.1122/1.4758001>
31. W. Wu, K. Zeng, B. Zhao, F. Duan, F. Jiang, New considerations on the determination of the apparent shear viscosity of polymer melt with micro capillary dies. *Polymers* **13**(24), 4451 (2021). <https://doi.org/10.3390/polym13244451>
32. P.J. Carreau, D.C.R. De Kee, R.P. Chhabra, 3- Rheometry, in *Rheology of Polymeric Systems*, ed. by P.J. Carreau, D.C.R. De Kee, R.P. Chhabra, 2nd edn., (Hanser, 2021), pp. 69–130

33. C.J. Pipe, T.S. Majmudar, G.H. McKinley, High shear rate viscometry. *Rheol. Acta* **47**(5), 621–642 (2008). <https://doi.org/10.1007/s00397-008-0268-1>
34. G. Bossis, O. Volkova, Y. Grasselli, O. Gueye, Discontinuous shear thickening in concentrated suspensions. *Philos. Trans. R. Soc. A Math. Phys. Eng. Sci.* **377**(2143), 20180211 (2019). <https://doi.org/10.1098/rsta.2018.0211>
35. M. Wyart, M.E. Cates, Discontinuous shear thickening without inertia in dense non-Brownian suspensions. *Phys. Rev. Lett.* **112**(9), 098302 (2014). <https://doi.org/10.1103/PhysRevLett.112.098302>
36. G. Bossis, Y. Grasselli, A. Cifrefo, O. Volkova, Tunable discontinuous shear thickening in capillary flow of MR suspensions. *J. Intell. Mater. Syst. Struct.* **32**(12), 1349–1357 (2020). <https://doi.org/10.1177/1045389X20959458>
37. S.R. Waitukaitis, H.M. Jaeger, Impact-activated solidification of dense suspensions via dynamic jamming fronts. *Nature* **487**(7406), 205–209 (2012). <https://doi.org/10.1038/nature11187>
38. I.R. Peters, H.M. Jaeger, Quasi-2D dynamic jamming in cornstarch suspensions: Visualization and force measurements. *Soft Matter* **10**(34), 6564–6570 (2014). <https://doi.org/10.1039/C4SM00864B>
39. R. Maharjan, S. Mukhopadhyay, B. Allen, T. Storz, E. Brown, Constitutive relation for the system-spanning dynamically jammed region in response to impact of cornstarch and water suspensions. *Phys. Rev. E* **97**(5), 052602 (2018). <https://doi.org/10.1103/PhysRevE.97.052602>
40. S. Gürgen, M.A. Sofuoğlu, M.C. Kuşhan, Rheological compatibility of multi-phase shear thickening fluid with a phenomenological model. *Smart Mater. Struct.* **28**(3), 035027 (2019). <https://doi.org/10.1088/1361-665X/ab018c>
41. M. Wei, L. Sun, P. Qi, C. Chang, C. Zhu, Continuous phenomenological modeling for the viscosity of shear thickening fluids. *Nanomater. Nanotechnol.* **8**, 1847980418786551 (2018). <https://doi.org/10.1177/1847980418786551>
42. A. Ghosh, I. Chauhan, A. Majumdar, B.S. Butola, Influence of cellulose nanofibers on the rheological behavior of silica-based shear-thickening fluid. *Cellulose* **24**(10), 4163–4171 (2017). <https://doi.org/10.1007/s10570-017-1440-5>
43. M. Wei, K. Lin, L. Sun, Shear thickening fluids and their applications. *Mater. Des.* **216**, 110570 (2022) <https://www.sciencedirect.com/science/article/pii/S0264127522001915>
44. K. Lin, J. Qi, H. Liu, M. Wei, H. Peng, A phenomenological theory-based viscosity model for shear thickening fluids. *Mater. Res. Express.* **9**, 015701 (2022)
45. J. David, P. Filip, A.A. Kharlamov, Empirical modelling of nonmonotonous behaviour of shear viscosity. *Adv. Mater. Sci. Eng.* **2013**, 658187 (2013). <https://doi.org/10.1155/2013/658187>
46. M. Wei, K. Lin, Q. Guo, H. Sun, Characterization and performance analysis of a shear thickening fluid damper. *Meas. Control* **52**, 002029401881954 (2019)
47. F.J. Galindo-Rosales, F.J. Rubio-Hernández, A. Sevilla, R.H. Ewoldt, How Dr. Malcom M. cross may have tackled the development of “an apparent viscosity function for shear thickening fluids”. *J. Non-Newtonian Fluid Mech.* **166**(23), 1421–1424 (2011) <https://www.sciencedirect.com/science/article/pii/S0377025711002011>
48. T. Shende, V.J. Niasar, M. Babaei, An empirical equation for shear viscosity of shear thickening fluids. *J. Mol. Liq.* **325**, 115220 (2021) <https://www.sciencedirect.com/science/article/pii/S0167732220374626>
49. S. Khandavalli, J.A. Lee, M. Pasquali, J.P. Rothstein, The effect of shear-thickening on liquid transfer from an idealized gravure cell. *J. Non-Newtonian Fluid Mech.* **221**, 55–65 (2015) <https://www.sciencedirect.com/science/article/pii/S0377025715000592>
50. R. Maharjan, E. Brown, Giant deviation of a relaxation time from generalized Newtonian theory in discontinuous shear thickening suspensions. *Phys. Rev. Fluids.* **2**(12), 123301 (2017). <https://doi.org/10.1103/PhysRevFluids.2.123301>
51. F.J. Rubio-Hernández, J.H. Sánchez-Toro, N.M. Páez-Flor, Testing shear thinning/thixotropy and shear thickening/antithixotropy relationships in a fumed silica suspension. *J. Rheol.* **64**(4), 785–797 (2020). <https://doi.org/10.1122/1.5131852>

52. V. Rathee, D.L. Blair, J.S. Urbach, Localized stress fluctuations drive shear thickening in dense suspensions. *Proc. Natl. Acad. Sci.* **114**(33), 8740–8745 (2017). <https://doi.org/10.1073/pnas.1703871114>
53. M. Tassieri, J. Ramírez, N.C. Karayiannis, S.K. Sukumaran, Y. Masubuchi, I-Rheo GT: Transforming from time to frequency domain without artifacts. *Macromolecules* **51**(14), 5055–5068 (2018). <https://doi.org/10.1021/acs.macromol.8b00447>
54. R. Rivas-Barbosa, M.A. Escobedo-Sánchez, M. Tassieri, M. Laurati, I-Rheo: Determining the linear viscoelastic moduli of colloidal dispersions from step-stress measurements. *Phys. Chem. Chem. Phys.* **22**(7), 3839–3848 (2020). <https://doi.org/10.1039/C9CP06191F>
55. F. Juliusburger, A. Pirquet, Thixotropy and rheopecty of V2O5-sols. *Trans. Faraday Soc.* **32**, 445–452 (1936). <https://doi.org/10.1039/TF9363200445>
56. J. Mewis, Thixotropy - a general review. *J. Non-Newtonian Fluid Mech.* **6**(1), 1–20 (1979) <https://www.sciencedirect.com/science/article/pii/0377025779870019>
57. J. Lyklema, H. Van Olphen, Terminology and symbols in colloid and surface chemistry part 1.13. Definitions, terminology and symbols for rheological properties. *Pure Appl. Chem.* **51**(5), 1213–1218 (1979). <https://doi.org/10.1351/pac197951051213>
58. R.G. Larson, Y. Wei, A review of thixotropy and its rheological modeling. *J. Rheol.* **63**(3), 477–501 (2019). <https://doi.org/10.1122/1.5055031>
59. J.H. Cho, A.H. Griese, I.R. Peters, I. Bischofberger, Lasting effects of discontinuous shear thickening in cornstarch suspensions upon flow cessation. *Phys. Rev. Fluids.* **7**(6), 063302 (2022). <https://doi.org/10.1103/PhysRevFluids.7.063302>
60. Z. Pan, H. de Cagny, B. Weber, D. Bonn, S -shaped flow curves of shear thickening suspensions: Direct observation of frictional rheology. *Phys. Rev. E* **92**(3), 032202 (2015). <https://doi.org/10.1103/PhysRevE.92.032202>
61. R.P. Chhabra, J.F. Richardson, Chapter 1 - Non-Newtonian fluid behaviour, in *Non-Newtonian Flow in the Process Industries*, ed. by R.P. Chhabra, J.F. Richardson, (Butterworth-Heinemann, Oxford, 1999), pp. 1–36
62. F.J. Galindo-Rosales, F.J. Rubio-Hernández, Transient study on the shear thickening behaviour of surface modified Fumed silica suspensions in polypropylene glycol. *AIP Conf. Proc.* **1027**(1), 686–688 (2008). <https://doi.org/10.1063/1.2964809>
63. Y. Wei, M.J. Solomon, R.G. Larson, A multimode structural kinetics constitutive equation for the transient rheology of thixotropic elasto-viscoplastic fluids. *J. Rheol.* **62**(1), 321–342 (2017). <https://doi.org/10.1122/1.4996752>
64. X. Cheng, H. McCoy Jonathan, N. Israelachvili Jacob, I. Cohen, Imaging the microscopic structure of shear thinning and thickening colloidal suspensions. *Science* **333**(6047), 1276–1279 (2011). <https://doi.org/10.1126/science.1207032>
65. V. Rathee, D.L. Blair, J.S. Urbach, Dynamics and memory of boundary stresses in discontinuous shear thickening suspensions during oscillatory shear. *Soft Matter* **17**(5), 1337–1345 (2021). <https://doi.org/10.1039/D0SM01917H>
66. G. Ovarlez, A. Vu Nguyen Le, W.J. Smit, A. Fall, R. Mari, G. Chatté, et al., Density waves in shear-thickening suspensions. *Sci. Adv.* **6**(16), eaay 5589 (2020). <https://doi.org/10.1126/sciadv.aay5589>
67. A. Gauthier, M. Pruvost, O. Gamache, A. Colin, A new pressure sensor array for normal stress measurement in complex fluids. *J. Rheol.* **65**(4), 583–594 (2021). <https://doi.org/10.1122/8.0000249>
68. B. Saint-Michel, T. Gibaud, S. Manneville, Uncovering instabilities in the spatiotemporal dynamics of a shear-thickening Cornstarch suspension. *Phys. Rev. X* **8**(3), 031006 (2018). <https://doi.org/10.1103/PhysRevX.8.031006>
69. J. Mewis, G. Biebaut, Shear thickening in steady and superposition flows effect of particle interaction forces. *J. Rheol.* **45**(3), 799–813 (2001). <https://doi.org/10.1122/1.1359761>
70. H. Ramli, N.F.A. Zainal, M. Hess, C.H. Chan, Basic principle and good practices of rheology for polymers for teachers and beginners. *Chemistry Teacher International* **4**(4), 307–326 (2022). <https://doi.org/10.1515/cti-2022-0010>

71. K. Hyun, S.H. Kim, K.H. Ahn, S.J. Lee, Large amplitude oscillatory shear as a way to classify the complex fluids. *J. Nonnewton Fluid Mech* **107**, 51–65 (2002). [https://doi.org/10.1016/S0377-0257\(02\)00141-6](https://doi.org/10.1016/S0377-0257(02)00141-6)
72. H.M. Laun, R. Bung, F. Schmidt, Rheology of extremely shear thickening polymer dispersions (passively viscosity switching fluids). *J. Rheol.* **35**(6), 999–1034 (1991) <https://www.scopus.com/inward/record.uri?eid=2-s2.0-76149128078&doi=10.1122%2f1.550257&partnerID=40&md5=0debbc1882216f1a2b2f19ea4ffbc7bc>
73. W.H. Boersma, J. Laven, H.N. Stein, Viscoelastic properties of concentrated shear-thickening dispersions. *J. Colloid Interface Sci.* **149**(1), 10–22 (1992) <https://www.sciencedirect.com/science/article/pii/S002197979290385Y>
74. S.R. Raghavan, S.A. Khan, Shear-thickening response of Fumed silica suspensions under steady and oscillatory shear. *J. Colloid Interface Sci.* **185**(1), 57–67 (1997) <https://www.sciencedirect.com/science/article/pii/S0021979796945816>
75. F. Yziquel, P.J. Carreau, P.A. Tanguy, Non-linear viscoelastic behavior of fumed silica suspensions. *Rheol. Acta* **38**(1), 14–25 (1999). <https://doi.org/10.1007/s003970050152>
76. Y.S. Lee, N.J. Wagner, Dynamic properties of shear thickening colloidal suspensions. *Rheol. Acta* **42**(3), 199–208 (2003). <https://doi.org/10.1007/s00397-002-0290-7>
77. C. Fischer, C.J.G. Plummer, V. Michaud, P.-E. Bourban, J.-A.E. Månson, Pre- and post-transition behavior of shear-thickening fluids in oscillating shear. *Rheol. Acta* **46**(8), 1099–1108 (2007). <https://doi.org/10.1007/s00397-007-0202-y>
78. L. Chang, K. Friedrich, A.K. Schlarb, R. Tanner, L. Ye, Shear-thickening behaviour of concentrated polymer dispersions under steady and oscillatory shear. *J. Mater. Sci.* **46**(2), 339–346 (2011). <https://doi.org/10.1007/s10853-010-4817-5>
79. S. Khandavalli, J.P. Rothstein, Large amplitude oscillatory shear rheology of three different shear-thickening particle dispersions. *Rheol. Acta* **54**(7), 601–618 (2015). <https://doi.org/10.1007/s00397-015-0855-x>
80. J. Lee, Z. Jiang, J. Wang, A.R. Sandy, S. Narayanan, X.-M. Lin, Unraveling the role of order-to-disorder transition in shear thickening suspensions. *Phys. Rev. Lett.* **120**(2), 028002 (2018). <https://doi.org/10.1103/PhysRevLett.120.028002>
81. D. Doraiswamy, A.N. Mujumdar, I. Tsao, A.N. Beris, S.C. Danforth, A.B. Metzner, The Cox–Merz rule extended: A rheological model for concentrated suspensions and other materials with a yield stress. *J. Rheol.* **35**(4), 647–685 (1991). <https://doi.org/10.1122/1.550184>
82. Q. Zhao, Y. He, H. Yao, B. Wen, Dynamic performance and mechanical model analysis of a shear thickening fluid damper. *Smart Mater. Struct.* **27**(7), 075021 (2018). <https://doi.org/10.1088/1361-665X/aac23f>
83. X.Z. Zhang, W.H. Li, X.L. Gong, The rheology of shear thickening fluid (STF) and the dynamic performance of an STF-filled damper. *Smart Mater. Struct.* **17**(3), 035027 (2008). <https://doi.org/10.1088/0964-1726/17/3/035027>
84. K. Lin, A. Zhou, H. Liu, Y. Liu, C. Huang, Shear thickening fluid damper and its application to vibration mitigation of stay cable. *Structure* **26**, 214–223 (2020) <https://www.sciencedirect.com/science/article/pii/S2352012420301727>
85. Q. Zhao, J. Yuan, H. Jiang, H. Yao, B. Wen, Vibration control of a rotor system by shear thickening fluid dampers. *J. Sound Vib.* **494**, 115883 (2021) <https://www.sciencedirect.com/science/article/pii/S0022460X20307203>
86. F.J. Rubio-Hernández, Testing a shear-thickening fumed silica suspension with parallel superposition rheology. *J. Mol. Liq.* **365**, 120179 (2022) <https://www.sciencedirect.com/science/article/pii/S0167732222017184>
87. P. Moldenaers, J. Mewis, On the nature of viscoelasticity in polymeric liquid crystals. *J. Rheol.* **37**(2), 367–380 (1993). <https://doi.org/10.1122/1.550448>
88. BA de L Costello. Parallel superposition rheology of an associatively thickened latex. TA Instruments applications note RH-060
89. Tianhong Chen. Parallel Superposition Studies on Paint Using An ARES-G2 Rheometer. TA Instruments applications note RH093

90. K. Niedzwiedz, H. Buggisch, N. Willenbacher, Extensional rheology of concentrated emulsions as probed by capillary breakup elongational rheometry (CaBER). *Rheol. Acta* **49**(11), 1103–1116 (2010). <https://doi.org/10.1007/s00397-010-0477-2>
91. L. Martinie, H. Buggisch, N. Willenbacher, Apparent elongational yield stress of soft matter. *J. Rheol.* **57**(2), 627–646 (2013). <https://doi.org/10.1122/1.4789785>
92. F.J. Galindo-Rosales, J.P. Segovia-Gutiérrez, F.T. Pinho, M.A. Alves, J. de Vicente, Extensional rheometry of magnetic dispersions. *J. Rheol.* **59**(1), 193–209 (2014). <https://doi.org/10.1122/1.4902356>
93. S.H. Sadek, H.H. Najafabadi, F.J. Galindo-Rosales, Capillary breakup extensional magnetorheometry. *J. Rheol.* **64**(1), 55–65 (2019). <https://doi.org/10.1122/1.5115460>
94. S.H. Sadek, H.H. Najafabadi, F.J. Galindo-Rosales, Capillary breakup extensional electrorheometry (CaBEER). *J. Rheol.* **64**(1), 43–54 (2019). <https://doi.org/10.1122/1.5116718>
95. J.H. García-Ortiz, F.J. Galindo-Rosales, Extensional Magnetorheology as a tool for optimizing the formulation of ferrofluids in oil-spill clean-up processes. *PRO* **8**(5) (2020)
96. J.M. Nunes, F.J. Galindo-Rosales, L. Campo-Deaño, Extensional Magnetorheology of viscoelastic human blood analogues loaded with magnetic particles. *Materials* **14**(22), 6930 (2021)
97. H.C.H. Ng, A. Corker, E. García-Tuñón, R.J. Poole, GO CaBER: Capillary breakup and steady-shear experiments on aqueous graphene oxide (GO) suspensions. *J. Rheol.* **64**(1), 81–93 (2019). <https://doi.org/10.1122/1.5109016>
98. E. White, M. Chellamuthu, J. Rothstein, Extensional rheology of a shear-thickening corn-starch and water suspension. *Rheol. Acta* **49**, 119–129 (2009)
99. M. Chellamuthu, E. Arndt, J. Rothstein, Extensional rheology of shear-thickening nanoparticle suspensions. *Soft Matter* **5**, 2117–2124 (2009)
100. M.I. Smith, R. Besseling, M.E. Cates, V. Bertola, Dilatancy in the flow and fracture of stretched colloidal suspensions. *Nat. Commun.* **1**(1), 114 (2010). <https://doi.org/10.1038/ncomms1119>
101. S. Khandavalli, J.P. Rothstein, Extensional rheology of shear-thickening fumed silica nanoparticles dispersed in an aqueous polyethylene oxide solution. *J. Rheol.* **58**(2), 411–431 (2014). <https://doi.org/10.1122/1.4864620>
102. M. Roché, H. Kellay, H.A. Stone, Heterogeneity and the role of normal stresses during the extensional thinning of non-Brownian shear-thickening fluids. *Phys. Rev. Lett.* **107**(13), 134503 (2011). <https://doi.org/10.1103/PhysRevLett.107.134503>
103. S.L. Anna, G.H. McKinley, Effect of a controlled pre-deformation history on extensional viscosity of dilute polymer solutions. *Rheol. Acta* **47**(8), 841–859 (2008). <https://doi.org/10.1007/s00397-007-0253-0>
104. J.R. Morillas, J. de Vicente, Magnetorheology: A review. *Soft Matter* **16**(42), 9614–9642 (2020). <https://doi.org/10.1039/D0SM01082K>
105. P. Sheng, W. Wen, Electrorheological fluids: Mechanisms, dynamics, and microfluidics applications. *Annu. Rev. Fluid Mech.* **44**(1), 143–174 (2011). <https://doi.org/10.1146/annurev-fluid-120710-101024>
106. M. Terkel, J. de Vicente, Magnetorheology of exotic magnetic mesostructures generated under triaxial unsteady magnetic fields. *Smart Mater. Struct.* **30**(1), 014005 (2020). <https://doi.org/10.1088/1361-665X/abcca3>
107. M. Terkel, J. Tajuelo, J. de Vicente, Enhancing magnetorheology with precession magnetic fields. *J. Rheol.* **66**(1), 67–78 (2021). <https://doi.org/10.1122/8.0000356>
108. Transport Phenomena Research Center. Smart Fluids: CEFT; Available from <https://ceft.fe.up.pt/fluids/smart-fluids/>
109. X. Zhang, W. Li, X.L. Gong, Study on magnetorheological shear thickening fluid. *Smart Mater. Struct.* **17**(1), 015051 (2008). <https://doi.org/10.1088/0964-1726/17/1/015051>
110. C. Qian, Y. Tian, Z. Fan, Z. Sun, Z. Ma, Investigation on rheological characteristics of magnetorheological shear thickening fluids mixed with micro CBN abrasive particles. *Smart Mater. Struct.* **31**(9), 095004 (2022). <https://doi.org/10.1088/1361-665X/ac7bbd>

111. Y. Ming, X.M. Huang, D.D. Zhou, Q. Zeng, H.Y. Li, Rheological properties of magnetic field-assisted thickening fluid and high-efficiency spherical polishing of ZrO₂ ceramics. *Int. J. Adv. Manuf. Technol.* **121**(1), 1049–1061 (2022). <https://doi.org/10.1007/s00170-022-09344-4>
112. J. Yang, S. Sun, W. Li, H. Du, G. Alici, M. Nakano, Development of a linear damper working with magnetorheological shear thickening fluids. *J. Intell. Mater. Syst. Struct.* **26**(14), 1811–1817 (2015). <https://doi.org/10.1177/1045389X15577653>
113. A. Rendos, S. Woodman, K. McDonald, T. Ranzani, K.A. Brown, Shear thickening prevents slip in magnetorheological fluids. *Smart Mater. Struct.* **29**(7), 07LT2 (2020). <https://doi.org/10.1088/1361-665X/ab8b2e>
114. G. Bossis, Y. Grasselli, A. Meunier, O. Volkova, Outstanding magnetorheological effect based on discontinuous shear thickening in the presence of a superplasticizer molecule. *Appl. Phys. Lett.* **109**(11), 111902 (2016). <https://doi.org/10.1063/1.4962467>
115. F. Vereda, J.P. Segovia-Gutiérrez, J. de Vicente, R. Hidalgo-Alvarez, Faceted particles: An approach for the enhancement of the elasticity and the yield-stress of magnetorheological fluids. *Appl. Phys. Lett.* **108**(21), 211904 (2016). <https://doi.org/10.1063/1.4952394>
116. S.S. Shenoy, N.J. Wagner, J.W. Bender, E-FiRST: Electric field responsive shear thickening fluids. *Rheol. Acta* **42**(4), 287–294 (2003). <https://doi.org/10.1007/s00397-002-0289-0>
117. Y. Tian, M. Zhang, J. Jiang, N. Pesika, H. Zeng, J. Israelachvili, et al., Reversible shear thickening at low shear rates of electrorheological fluids under electric fields. *Phys. Rev. E* **83**(1), 011401 (2011). <https://doi.org/10.1103/PhysRevE.83.011401>
118. J. Jiang, Y. Liu, L. Shan, X. Zhang, Y. Meng, H.J. Choi, et al., Shear thinning and shear thickening characteristics in electrorheological fluids. *Smart Mater. Struct.* **23**(1), 015003 (2013). <https://doi.org/10.1088/0964-1726/23/1/015003>
119. S. Gürgen, M.A. Sofuoğlu, Vibration attenuation of sandwich structures filled with shear thickening fluids. *Compos. Part B* **186**, 107831 (2020) <https://www.sciencedirect.com/science/article/pii/S1359836819355131>
120. S. Gürgen, M.A. Sofuoğlu, Experimental investigation on vibration characteristics of shear thickening fluid filled CFRP tubes. *Compos. Struct.* **226**, 111236 (2019) <https://www.sciencedirect.com/science/article/pii/S0263822319316988>
121. L. Sun, M. Wei, J. Zhu, Low velocity impact performance of fiber-reinforced polymer impregnated with shear thickening fluid. *Polym. Test.* **96**, 107095 (2021) <https://www.sciencedirect.com/science/article/pii/S0142941821000453>
122. H. Taş, I.F. Soykok, Investigation of the low velocity impact behaviour of shear thickening fluid impregnated Kevlar, hybrid (Kevlar/carbon) and carbon fabrics. *Fibers Polym.* **22**(9), 2626–2634 (2021). <https://doi.org/10.1007/s12221-021-1358-2>
123. F. Pinto, M. Meo, Design and manufacturing of a novel shear thickening fluid composite (STFC) with enhanced out-of-plane properties and damage suppression. *Appl. Compos. Mater.* **24**(3), 643–660 (2017). <https://doi.org/10.1007/s10443-016-9532-1>
124. E. Selver, Impact and damage tolerance of shear thickening fluids-impregnated carbon and glass fabric composites. *J. Reinf. Plast. Compos.* **38**(14), 669–688 (2019). <https://doi.org/10.1177/0731684419842648>
125. F. Galindo-Rosales, S. Martínez-Aranda, L. Campo-Deaño, Cork STF_μfluidics – A novel concept for the development of eco-friendly light-weight energy absorbing composites. *Mater. Des.* **82** (2015)
126. A. Haris, H.P. Lee, V.B.C. Tan, An experimental study on shock wave mitigation capability of polyurea and shear thickening fluid based suspension pads. *Def. Technol.* **14**(1), 12–18 (2018) <https://www.sciencedirect.com/science/article/pii/S2214914717301150>
127. M.A. Dawson, Composite plates with a layer of fluid-filled, reticulated foam for blast protection of infrastructure. *Int. J. Impact Eng.* **36**(10), 1288–1295 (2009) <https://www.sciencedirect.com/science/article/pii/S0734743X09000621>
128. M.A. Dawson, G.H. McKinley, L.J. Gibson, The dynamic compressive response of open-cell foam impregnated with a Newtonian fluid. *J. Appl. Mech.* **75**(4), 041015 (2008). <https://doi.org/10.1115/1.2912940>

129. S. Gürgen, M.C. Kuşhan, The ballistic performance of aramid based fabrics impregnated with multi-phase shear thickening fluids. *Polym. Test.* **64**, 296–306 (2017) <https://www.sciencedirect.com/science/article/pii/S0142941817313478>
130. A.F. Ávila, A.M. de Oliveira, S.G. Leão, M.G. Martins, Aramid fabric/nano-size dual phase shear thickening fluid composites response to ballistic impact. *Compos. A: Appl. Sci. Manuf.* **112**, 468–474 (2018) <https://www.sciencedirect.com/science/article/pii/S1359835X18302689>
131. M. Hasanzadeh, V. Mottaghtalab, The role of shear-thickening fluids (STFs) in ballistic and stab-resistance improvement of flexible Armor. *J. Mater. Eng. Perform.* **23**(4), 1182–1196 (2014). <https://doi.org/10.1007/s11665-014-0870-6>
132. K. Yu, H. Cao, K. Qian, L. Jiang, *Li HJF* (Europe TiE, Synthesis and Stab Resistance of Shear Thickening Fluid (STF) Impregnated Glass Fabric Composites, 2012)
133. M.J. Decker, C.J. Halbach, C.H. Nam, N.J. Wagner, E.D. Wetzel, Stab resistance of shear thickening fluid (STF)-treated fabrics. *Compos. Sci. Technol.* **67**(3), 565–578 (2007) <https://www.sciencedirect.com/science/article/pii/S0266353806002983>
134. S. Gürgen, T. Yıldız, Stab resistance of smart polymer coated textiles reinforced with particle additives. *Compos. Struct.* **235**, 111812 (2020) <https://www.sciencedirect.com/science/article/pii/S0263822319337614>
135. S. Gürgen, M.C. Kuşhan, The stab resistance of fabrics impregnated with shear thickening fluids including various particle size of additives. *Compos. A: Appl. Sci. Manuf.* **94**, 50–60 (2017) <https://www.sciencedirect.com/science/article/pii/S1359835X1630447X>
136. J.M. Dealy, A.J. Giacomin, Sliding plate and sliding cylinder rheometers, in *Rheological Measurement*, ed. by A.A. Collyer, D.W. Clegg, (Springer Netherlands, Dordrecht, 1998), pp. 237–259
137. A.J. Giacomin, T. Samurkas, J.M. Dealy, A novel sliding plate rheometer for molten plastics. *Polym. Eng. Sci.* **29**(8), 499–504 (1989). <https://doi.org/10.1002/pen.760290803>
138. K.C. Ortman, N. Agarwal, A.P.R. Eberle, D.G. Baird, P. Wapperom, G.A. Jeffrey, Transient shear flow behavior of concentrated long glass fiber suspensions in a sliding plate rheometer. *J. Non-Newtonian Fluid Mech.* **166**(16), 884–895 (2011) <https://www.sciencedirect.com/science/article/pii/S0377025711000930>
139. J. Xu, S. Costeux, J.M. Dealy, M.N. De Decker, Use of a sliding plate rheometer to measure the first normal stress difference at high shear rates. *Rheol. Acta* **46**(6), 815–824 (2007). <https://doi.org/10.1007/s00397-006-0156-5>
140. C. Clasen, G.H. McKinley, Gap-dependent microrheometry of complex liquids. *J. Non-Newtonian Fluid Mech.* **124**(1), 1–10 (2004) <https://www.sciencedirect.com/science/article/pii/S0377025704002381>
141. D. Moon, A.J. Bur, K.B. Migler, Multi-sample micro-slit rheometry. *J. Rheol.* **52**(5), 1131–1142 (2008). <https://doi.org/10.1122/1.2955511>
142. T. Athanasiou, G.K. Auernhammer, D. Vlassopoulos, G. Petekidis, A high-frequency piezoelectric rheometer with validation of the loss angle measuring loop: Application to polymer melts and colloidal glasses. *Rheol. Acta* **58**(9), 619–637 (2019). <https://doi.org/10.1007/s00397-019-01163-x>
143. B. Schroyen, D. Vlassopoulos, P. Van Puyvelde, J. Vermant, Bulk rheometry at high frequencies: A review of experimental approaches. *Rheol. Acta* **59**(1), 1–22 (2020). <https://doi.org/10.1007/s00397-019-01172-w>
144. C.A.M. Verbaan, G.W.M. Peters, M. Steinbuch, Linear viscoelastic fluid characterization of ultra-high-viscosity fluids for high-frequency damper design. *Rheol. Acta* **54**(8), 667–677 (2015). <https://doi.org/10.1007/s00397-015-0862-y>
145. R.A. Secco, M. Kostic, J.R. de Bruyn, Fluid viscosity measurement, in *Measurement IaSH*, ed. by J.G. Webster, H. Eren, (Imprint CRC Press, 2014) p. 46-1: 31
146. J.J. Bikerman, A penetrovicometer for very viscous liquids. *J. Colloid Sci.* **3**(2), 75–85 (1948) <https://www.sciencedirect.com/science/article/pii/0095852248900592>

147. F. Koran, J.M. Dealy, A high pressure sliding plate rheometer for polymer melts. *J. Rheol.* **43**(5), 1279–1290 (1999). <https://doi.org/10.1122/1.551046>
148. A. Perrot, D. Rangeard, Y. Mélinge, Prediction of the Ram extrusion force of cement-based materials. *Appl. Rheol.* **24**(5), 34–40 (2014). <https://doi.org/10.3933/applrheol-24-53320>
149. K.D. Dolan, J.F. Steffe, R.G. Morgan, Back extrusion and simulation of viscosity development during starch gelatinization. *J. Food Process Eng.* **11**(2), 79–101 (1989). <https://doi.org/10.1111/j.1745-4530.1989.tb00023.x>
150. G.H. Brusewitz, H. Yu, Back extrusion method for determining properties of mustard slurry. *J. Food Eng.* **27**(3), 259–265 (1996) <https://www.sciencedirect.com/science/article/pii/0260877495000089>
151. K. Autio, T. Kuuva, K. Roininen, L. Lähteenmäki, Rheological properties, microstructure and sensory perception of high-amylose starch-pectin mixed gels. *J. Texture Stud.* **33**(6), 473–486 (2002). <https://doi.org/10.1111/j.1745-4603.2002.tb01362.x>
152. F. Nasaruddin, N.L. Chin, Y.A. Yusof, Effect of processing on instrumental textural properties of traditional Dodol using back extrusion. *Int. J. Food Prop.* **15**(3), 495–506 (2012). <https://doi.org/10.1080/10942912.2010.491932>
153. T.L. Smith, J.D. Ferry, F.W. Schrepf, Measurements of the mechanical properties of polymer solutions by electromagnetic transducers. *J. Appl. Phys.* **20**(2), 144–153 (1949). <https://doi.org/10.1063/1.1698326>
154. T. Hoshino, Analysis of viscosity measurements obtained using the short back extrusion method. Part 1: Theory of short back extrusion in viscometry. *J. Texture Stud.* **51**(2), 201–213 (2020). <https://doi.org/10.1111/jtxs.12501>
155. T. Hoshino, Analysis of viscosity measurements obtained using the short back extrusion method. Part 2: Verification of short back extrusion in viscometry. *J. Texture Stud.* **51**(2), 214–224 (2020). <https://doi.org/10.1111/jtxs.12510>
156. T. Hoshino, Analysis of the flow properties of a Herschel–Bulkley fluid using short back extrusion viscometry and considering time-dependent and stress growth behaviors. *Rheol. Acta* **59**(11), 809–819 (2020). <https://doi.org/10.1007/s00397-020-01243-3>
157. A.S. Lim, S.L. Lopatnikov, N.J. Wagner, J.W. Gillespie, Investigating the transient response of a shear thickening fluid using the split Hopkinson pressure bar technique. *Rheol. Acta* **49**(8), 879–890 (2010). <https://doi.org/10.1007/s00397-010-0463-8>
158. N. Asija, H. Chouhan, S.A. Gebremeskel, N. Bhatnagar, High strain rate characterization of shear thickening fluids using Split Hopkinson pressure bar technique. *Int. J. Impact Eng.* **110**, 365–370 (2017) <https://www.sciencedirect.com/science/article/pii/S0734743X16306534>
159. Z. Tan, J. Ge, H. Zhang, P. Zhai, W. Li, Dynamic response of shear thickening fluid reinforced with SiC nanowires under high strain rates. *Appl. Phys. Lett.* **111**(3), 031902 (2017). <https://doi.org/10.1063/1.4994066>
160. Y. Guo, Y. Wei, J. Zou, C. Huang, X. Wu, Z. Liu, et al., Impact and usage of the shear thickening fluid (STF) material in damping vibration of bolted flange joints. *Smart Mater. Struct.* **28**(9), 095005 (2019). <https://doi.org/10.1088/1361-665X/aaef6c>
161. A. Azimi, G.M. Owolabi, H. Fallahdoost, N. Kumar, G. Warner, High strain rate behavior of ultrafine grained AA2519 processed via multi axial cryogenic forging. *Metals* **9**(2), 115 (2019)
162. A.S. Lim, S.L. Lopatnikov, J.W. Gillespie, Development of the split-Hopkinson pressure bar technique for viscous fluid characterization. *Polym. Test.* **28**(8), 891–900 (2009) <https://www.sciencedirect.com/science/article/pii/S0142941809001342>
163. L.S. Madsen, M. Waleed, C.A. Casacio, A. Terrason, A.B. Stilgoe, M.A. Taylor, et al., Ultrafast viscosity measurement with ballistic optical tweezers. *Nat. Photonics* **15**(5), 386–392 (2021). <https://doi.org/10.1038/s41566-021-00798-8>
164. M. Zarei, J. Aalaie, Application of shear thickening fluids in material development. *J. Mater. Res. Technol.* **9**(5), 10411–10433 (2020) <https://www.sciencedirect.com/science/article/pii/S2238785420315489>